Modulational instability and unstable patterns in the discrete complex cubic Ginzburg-Landau equation with first and second neighbor couplings

Alidou Mohamadou,[1] A. Kenfack Jiotsa,[1] and T. C. Kofané[1,2]
[1]*Laboratoire de Mécanique, Département de Physique, Faculté des Sciences, Université de Yaoundé I, B.P. 812 Yaoundé, Cameroun*
[2]*The Abdus Salam International Centre for Theoretical Physics, P.O. Box 586 Strada Costiera, 11, I-34014 Trieste, Italy*
(Received 3 November 2003; revised manuscript received 18 April 2005; published 28 September 2005)

The generation of nonlinear modulated waves is investigated in the framework of hydrodynamics using a model of coupled oscillators. In this model, the separatrices between each pair of vortices may be viewed as individual oscillators and are described by a phenomenological one-dimensional discrete complex Ginzburg-Landau equation involving first- and second-nearest neighbor couplings. A theoretical approach based on the linear stability analysis predicts regions of modulational instability, governed by both the first and second-nearest neighbor couplings. From numerical investigations of different wave patterns that may be driven by the modulational instability, it appears that analytical predictions are correctly verified. For wave number in the unstable regions, an initial condition whose amplitude is slightly modulated breaks into a train of unstable patterns. This phenomenon agrees with the description of amplification of the spectral component of the perturbation and its harmonics, as well.

DOI: 10.1103/PhysRevE.72.036220 PACS number(s): 89.75.Kd, 05.45.−a, 89.75.Fb, 47.54.+r

I. INTRODUCTION

A well-known mechanism of pattern formation is the modulational instability (MI) [1,2] of wave trains against weak perturbations. The realization of this instability spans a wide range of fields, from fluid dynamics [1] (where it is usually referred to as Benjamin-Feir instability) and nonlinear optics [3,4] to Plasma Physics [5]. One of the earliest contexts in which its significance was pointed out was the linear stability analysis of deep water waves [1]. The phenomenon involves both continuous and discrete systems and consists of the exponential growth of the amplitude of a (quasi)monochromatic wave propagating in a weak nonlinear dispersive medium, leading to a wave breakup in either space or time. Since this disintegration typically occurs in the same parameter region where bright solitons are observed, MI is considered, to some extent, as a precursor to the formation of solitons [6]. In particular, temporal MI has been observed in optical fibers [7] as well as its spatial counterpart, namely nonlinear Kerr [8], quadratic [9], and biased photorefractive [10] media with both coherent and partially coherent beams.

Recently, the behavior of nonlinear discrete systems has received considerable attention in fields like biology [11], optics [12], solid state physics [13], Bose-Einstein condensates [14], and hydrodynamics [15,16]. Linear properties of this class of systems are strongly modified and, as a result, their nonlinear response is known to exhibit features that are otherwise unlikely in the bulk/continuous regime [17]. In some cases, these systems can be described by discrete Ginzburg-Landau (DGL) models [15,16,18]. Since the pioneering work of Newell and Whitehead [19], as well as Segel [20], the complex Ginzburg-Landau model has gained interest over the last three decades in connection with its application in various branches of physics. This equation is rather general compared with the nonlinear Schrödinger equation, since it includes dispersive and nonlinear effects in both conservative and dissipative forms. Indeed, DGL models have been considered in the literature to describe many nonequilibrium phenomena in physical systems such as discrete solitons [21], arrays of a semiconductor laser in nonlinear optics [18], Taylor and frustrated vortices in hydrodynamics [15]. In this last context, a set of experiments have been performed in a linear array of vortices to characterize ordered states, and interesting phenomena have been observed such as short-wavelength instability [22], frustration [15], and spatiotemporal intermittency [23].

Experiments on a linear array of vortices in a shallow conducting fluid have been recently carried out by Willaime *et al.* [15,22]. These experiments were carried out on a cell of rectangular cross sections subjected to a magnetic field. The cell is filled with a working fluid [24] and, in the bottom, a groove of 20 mm wide, with a variable depth, is machined. A steady electric current is imposed along the cell and the resulting magnetic force, which is spatially periodic, induces recirculating flows. Thus, a linear array of counter-rotating vortices whose number varies is obtained. As the electric current is increased, the system undergoes a transition from a state composed of counter-rotating vortices to a state where all the vortices have the same sign and are twice as large. The shadowgraph method is used to visualize the separatrices between the vortices; and, in turn, the spatiotemporal dynamics of the system. Due to the one-dimensional geometry and to the fact that vortices are produced by a forcing mechanism, the separatrices between the pair of vortices may be viewed as individual oscillators. Therefore, the system can be described theoretically by a chain of the coupled oscillator. The dynamics of individual oscillators is characterized by a complex number $W_n(t)$, i.e., an amplitude and a phase. Moreover, in agreement with the experiment, each of them results from a Hopf supercritical bifurcation. As concerns the interaction with the lattice, both linear and nonlinear first- and second-nearest-neighbor couplings have been taken into account. One thus gets the following phenomeno-

logical discrete complex Ginzburg-Landau (DCGL) equation [15] governing the evolution of the system:

$$\frac{dW_n}{dt} = \mu(1+ic_0)W_n - (1+ic_2)|W_n|^2W_n - (c_3+ic_4) \times(|W_{n-1}|^2+|W_{n+1}|^2)W_n + \varepsilon(1+ic_1)(W_{n+1}+W_{n-1}) + \varepsilon'(1+ic_1')(W_{n+2}+W_{n-2}), \quad (1)$$

where $\mu=(I-I_c)/I_c$. Here, μ is the control parameter of the system and I_c is the threshold value. When the threshold value is fixed, we can vary I, i.e., μ. The coefficients c_0, c_1, c_2, c_3, c_4, ε, c_1', and ε' are real. Parameters of the model have been measured for two depths 2 and 3 mm [23]. In the case where the fluid thickness is 2 mm, the second-nearest-neighbor couplings were effectively weak enough to give rise to frustration. Therefore as a rough approximation, frustration can be neglected at least for the lattice sizes considered. The equation governing the evolution of the system in this case is obtained from Eq. (1) with $\varepsilon'=0$. Frustrated states have been studied for many years in other contexts, such as spin glasses. However, it is only recently that their existence was proven in hydrodynamics [15]. In this last context, frustrated states are obtained for a depth of the groove of 3 mm, when ε' is negative and larger in absolute value than $\varepsilon/4$.

Like every nonlinear system, the model equation (1) can exhibit an instability that leads to self-induced modulation of an input plane wave with the subsequent generation of patterns. Modulational instability in discrete nonlinear Schrödinger-like lattices was first predicted in the first Brillouin zone [12]. Very recently, the first experimental observation of discrete modulational instability has been reported [25]. In view of the fact that discrete MI can occur in many physical systems, it is of fundamental importance to study it as it stands as a precursor phenomenon to the formation of discrete soliton [26]. It should be emphasized that discrete solitons are intrinsically highly localized [12].

Our purpose in this paper is to investigate the best conditions under which different wave patterns can emerge during the evolution of the wave, given an appropriate choice of the wave numbers in the system. The outline of the paper is as follows. In Sec. II, we examine MI as a function of the wave numbers in order to gain insight into the formation of patterns. We present numerical results for the MI of a plane wave in Sec. III and discuss their consistency with theoretical predictions. Section IV is devoted to concluding remarks.

II. LINEAR STABILITY ANALYSIS

To analyze the MI in the framework of the DCGL equation, we consider a first-order perturbation of harmonic waves [27] and seek the condition for their stability (instability). The DCGL equation is an appropriate amplitude equation to describe the pattern formation near a supercritical Hopf bifurcation [28,29] and, the slow dynamics near a supercritical transition to unidirectional traveling waves [28,29]. At the transition point, the most unstable mode is either an acoustical mode for a positive value of ε (where all the oscillators are in phase), or an optical mode for a negative value of ε (where each oscillator is out of phase with respect to its nearest neighbors). Since the temporal phase of such modes is defined only through an arbitrary constant, one can look for the instability which breaks the corresponding transition invariance. Oscillatory media near the Hopf bifurcation generally admit a family of traveling waves of the form

$$W_n(t) = W_0 \exp(i\theta_n), \quad \text{with} \quad \theta_n(t) = qna - \omega t, \quad (2)$$

where q denotes the wave number of the carrier wave. The frequency ω and the initial amplitude W_0 obey the nonlinear dispersion relation,

$$\omega = -\mu c_0 + (c_2+2c_4)|W_0|^2 - 2\varepsilon c_1\cos(qa) - 2\varepsilon' c_1'\cos(2qa),$$

$$(1+2c_3)|W_0|^2 = \mu + 2\varepsilon\cos(qa) + 2\varepsilon'\cos(2qa). \quad (3)$$

Oscillators n and $n+1$ are separated by the equilibrium distance a. To determine the parameter space in which the nonlinear plane waves are unstable, we carry out a linear stability analysis of these solutions by considering the perturbed solution as

$$W_n(t) = (W_0+b_n)\exp[i(\theta_n+\psi_n)], \quad (4)$$

where functions $b_n=b_n(t)$ and $\psi_n=\psi_n(t)$ are assumed to be small compared to the amplitude and phase of the carrier wave, respectively. After the substitution of Eq. (4) into Eq. (1), and linearization with respect to b_n and ψ_n, one obtains the following equation describing the evolution of the perturbations b_n and ψ_n,

$$\frac{\partial b_n}{\partial t} + iW_0\frac{\partial \psi}{\partial t} = -[1+2c_3+i(c_2+2c_4)]|W_0|^2(b_n+b_n^*) - (c_3+ic_4)(b_{n+1}+b_{n-1}-2b_n+b_{n+1}^*+b_{n-1}^*-2b_n^*) + \varepsilon(1+ic_1) \times\{[(b_{n+1}+b_{n-1}-2b_n)+iW_0(\psi_{n+1}+\psi_{n-1}-2\psi_n)]\cos(qa)+[i(b_{n+1}-b_{n-1})-W_0(\psi_{n+1}-\psi_{n-1})]\sin(qa)\} + \varepsilon'(1+ic_1')\{[(b_{n+2}+b_{n-2}-2b_n)+iW_0(\psi_{n+2}+\psi_{n-2}-2\psi_n)]\cos(2qa) + [i(b_{n+2}-b_{n-2})-W_0(\psi_{n+2}-\psi_{n-2})]\sin(2qa)\}, \quad (5)$$

in which (*) refers to complex conjugates of variables. Solutions of Eq. (5) that are a combination of progressive and regressive plane waves can be looked into

$$\begin{pmatrix} b_n \\ \psi_n \end{pmatrix} = \begin{pmatrix} b_1 & b_2 \\ \psi_1 & \psi_2 \end{pmatrix} \exp\begin{pmatrix} i(Qna+\Omega t) \\ -i(Qna+\Omega^* t) \end{pmatrix},$$

where b_1, b_2, ψ_1, and ψ_2 are real constants. The wave number Q and the frequency Ω characterize linear properties. The frequency Ω can be written as

$$\Omega = \Omega_r + i\sigma, \tag{6}$$

where Ω_r and σ are real constants, Ω_r can be chosen equal to ω by using the nonlinear dispersion relation (3). Inserting Eq. (6) into the expression of the perturbation helps in understanding the behavior of the system under the perturbation. Indeed, this operation gives

$$b_n(t) = b_1 e^{i[(\Omega_r+i\sigma)t+Qna]} + b_2 e^{-i[(\Omega_r-i\sigma)t+Qna]} = b_1 e^{-\sigma t} e^{i(\Omega_r t+Qna)} + b_2 e^{-\sigma t} e^{-i(\Omega_r t+Qna)}. \tag{7}$$

It can be noticed that $e^{-\sigma t}$ enters inside the amplitude of the perturbation. The asymptotic behavior of the perturbation is related to the sign of the constant σ. Hence, the real constant σ can be considered as a measure of the growth rate of the perturbation. Substituting this perturbation into Eq. (5) leads to a linear and homogeneous algebraic system (see Appendix (A1). As the emphasis is on nontrivial solutions, the determinant of the system has to be equal to zero. This can be translated into the following algebraic equation in σ:

$$\sigma^4 + K_3\sigma^3 + K_2\sigma^2 + K_1\sigma + K_0 = 0, \tag{8}$$

where coefficients $K_j (j=0,\ldots,3)$ are real and expressed in Appendix (A3). In order to obtain solutions of Eq. (8) and more precisely their nature (i.e., complex or real), successive transformations of this equation are carried out. If the transformation $\sigma \rightarrow \sigma + u$ (where u is equal to $K_3/4$) is applied in Eq. (8), the following equation is obtained:

$$\sigma^4 + K_2'\sigma^2 + K_1'\sigma + K_0' = 0. \tag{9}$$

Coefficients K_0', K_1', and K_2' depend on K_0, K_1, K_2, and K_3, and are expressed in Appendix (A4). From the Ferrari formulas [29], all solutions $\sigma_j (j=1,\ldots,4)$ of Eq. (9) can be written as follows:

$$\sigma_1 = [(\rho - K_2')^{1/2} + (\delta - K_2')^{1/2} + (\xi - K_2')^{1/2}]/2, \tag{10a}$$

$$\sigma_2 = [-(\rho - K_2')^{1/2} - (\delta - K_2')^{1/2} + (\xi - K_2')^{1/2}]/2, \tag{10b}$$

$$\sigma_3 = [(\rho - K_2')^{1/2} - (\delta - K_2')^{1/2} + (\xi - K_2')^{1/2}]/2, \tag{10c}$$

$$\sigma_4 = [(\rho - K_2')^{1/2} - (\delta - K_2')^{1/2} - (\xi - K_2')^{1/2}]/2, \tag{10d}$$

where ρ, δ, and ξ are the solutions of the following cubic equation $\sigma^3 - K_2'\sigma^2 - 4K_0'\sigma + 4K_2'K_0' - (K_1')^2 = 0$. Now, one applies the transformation $\sigma \rightarrow \sigma + u$, where u is now equal to $(K_2'/3)$ in the previous cubic equation to remove the term to the power two in σ. This operation leads to

$$\sigma^3 + K_1''\sigma + K_0'' = 0, \tag{11}$$

with K_0'', K_1'' real constants, which are defined in Appendix (A5). Equation (11) has three solutions $\sigma_{1(11)}, \sigma_{2(11)}, \sigma_{3(11)}$ defined as follows [29]:

$$\sigma_{1(11)} = (\rho - K_2'/3), \quad \sigma_{2(11)} = (\xi - K_2'/3),$$

$$\sigma_{3(11)} = (\delta - K_2'/3). \tag{12}$$

From the above stability analysis, the dispersion relation of the system has been obtained as a fourth-order polynomial, whose solutions are described in relation (8). In order to define the asymptotic behavior of the traveling wave solution, we need to specify the sign of the growth rates σ, i.e. the sign of solution (10). If the expression $[4(K_1'')^3 + 27(K_0'')^2]$ is positive, two solutions of relation (12) are complex and the other real. As a reminder, each solution of relation (10) depends on the three solutions $\sigma_{1(11)}, \sigma_{2(11)}, \sigma_{3(11)}$ [see Appendix (A6)]. Consequently, when one of these three solutions is complex, this implies that all solutions defined by Eq. (10) must be complex, i.e., the growth rate is a complex number. But, the real value of the growth rates as defined by Eq. (6) is the concern of this section. On the other hand, when the expression $[4(K_1'')^3 + 27(K_0'')^2]$ is negative, the three solutions $\sigma_{1(11)}, \sigma_{2(11)}, \sigma_{3(11)}$ are real. If one of them is less than $2K_2'/3$ [see Appendix (A6)], all the solutions defined by Eq. (10) will be complex, due to the presence of a negative number under the square root. But, if each of them is greater than $2K_2'/3$ [see Appendix (A6)], all the solutions defined by Eq. (10) are real. In this case, the growth rate exists as real constants. Therefore, this growth rate can be a positive or a negative number. For a given set of the model parameters and a particular value of wave numbers, we can specify its sign. Positive values of the growth rates σ means the stability of the system because of the vanishing long time $e^{-\sigma t}$. In this case, the system remains stable under the modulation. While its negative values are the signature of instability. The perturbation diverges without limit as the time t increases and the corresponding solution is said to be modulationally unstable. Because of the discreteness of the lattice, wave numbers q and Q that differ by 2π correspond to the same wave. Thus, the present study can be restricted to the first Brillouim zone $[-\pi, \pi]$. Finally, $[0, \pi]$ is considered, since only the direction of propagation is changing for $-q$ and $-Q$. Based upon the roots of Eq. (8), which is related to the dispersion relation, the results obtained for the stability diagram can be obtained either by the analytical solutions or numerically solving Eq. (8), and the results would be the same. But the stability diagram results presented here are obtained by numerical computation. With the above established criteria, the main features of the instability are highlighted in Fig. 1, where the stability diagram is plotted in a (Q,q) plane. The dark regions correspond to area of instability while the white are regions of stability. In these instability regions, at least one of the four growth rates $\sigma(q,Q)$ is negative $[\sigma(q,Q) < 0]$. As stated previously, when the second neighbor coupling coefficient is negative $(\varepsilon' < 0)$ and is larger in absolute value than $\varepsilon/4$, there is a competition be-

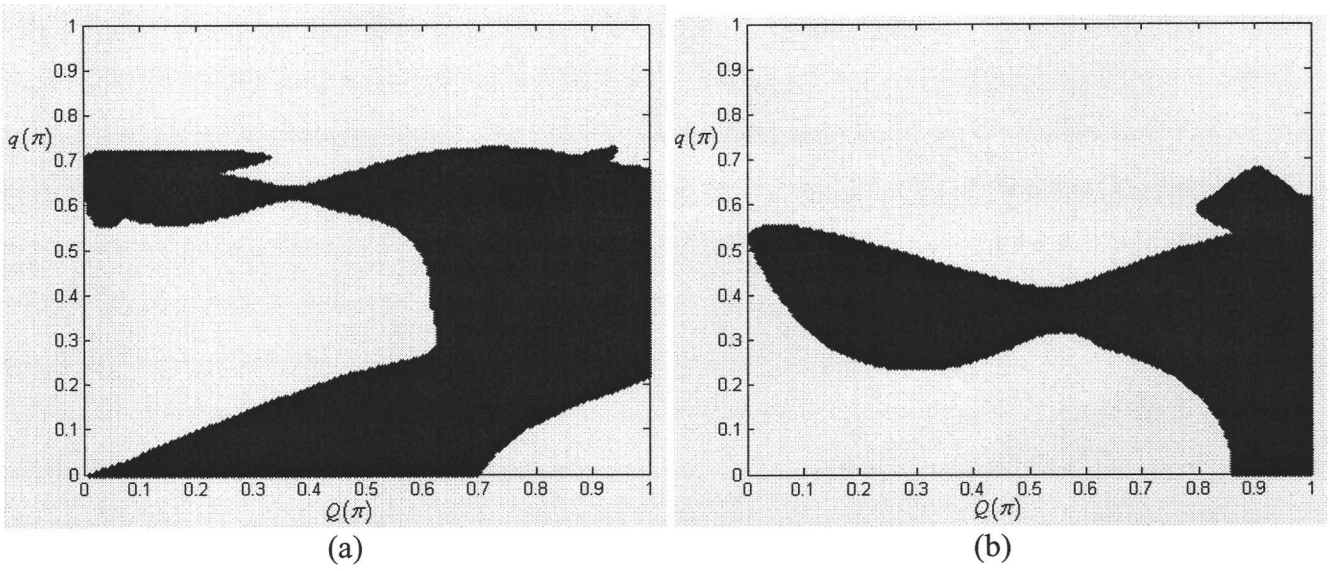

FIG. 1. (a) Frustrated regions of instability (black area) on the (q,Q) plane. $c_0=-0.11$, $c_1=0.22$, $c_2=-1.34$, $c_3=3.0$, $c_4=0.046$, $\varepsilon=0.23$, $c_1'=0.22$, $\varepsilon'=-0.23$, $\mu=0.25$. (b) Regions of instability (black area) on the (q,Q) plane in the absence of second neighbors coupling. The same parameters as in (a), but with $c_1'=0.0$ and $\varepsilon'=0.0$.

tween the first- and second-nearest-neighbor coupling. This competition gives rise to "frustrated states." Figure 1(a) presents the case of a frustrated modulational instability region plotted in the (Q,q) plane. The model parameters used are those measured by Willaime *et al.* [15]: $c_0=-0.11$, $c_1=0.22$, $c_2=-1.34$, $c_3=3.0$, $c_4=0.046$, $\varepsilon=0.23$, $c_1'=0.22$, $\varepsilon'=-0.23$, and $\mu=0.25$. It has been obtained that the area of instability region (black region) grows while increasing either μ or Ω_r [Ω_r can be chosen to be equal to ω by using the dispersion relation (3)]. However, plane waves with $q>0.7\pi$ are always stable with respect to any perturbation irrespective of the value of Q. One can also observe in Fig. 1(a) that, for long-wavelength (small Q) perturbations, a carrier wave with very small q is unstable, but is stable for a carrier wave with large q upper to the middle of the Brillouin zone. On the other hand, when restricting ourselves to nearest-neighbor coupling ($\varepsilon'=0$), the area of the instability region shrunk, as seen in Fig. 1(b). This figure indicates that a carrier wave with small q is stable to long-wavelength perturbations, but unstable against short-wavelength perturbations. This is different from what was reported in [30] for the monatomic Klein-Gordon chain that is also subject to discreteness effects and nearest neighbor coupling. In the Klein-Gordon chain, the small-Q region is always the unstable region as long as the instability occurs for the corresponding carrier wave, while the large-Q region is always the stable region.

A number of studies of various lattice dynamical models have shown that the existence of intrinsic localized modes is always accompanied by the instability of corresponding extended nonlinear plane waves [30–32]. Another main effect of modulational instability is the creation of localized pulses [33]. This is in agreement with the results presented above, which show that, for negative values of the growth rates σ, the system is unstable. Consequently, nonlinearity can induce the formation of localized patterns in the unstable region.

III. PROPAGATIVE PATTERNS OF THE MODEL EQUATION

According to the above analytical results based on a linear stability analysis, the stability of a nonlinear plane wave with wave number q modulated by a small-amplitude wave of wave number Q is determined by the dispersion relation (8). Linear stability analysis can determine the instability domain in parameter space and predict qualitatively how the amplitude of a modulation sideband evolves at the onset of the instability. However, such an analysis is based on the linearization around the unperturbed carrier wave, which is valid only when the amplitude of the perturbation is small in comparison with that of the carrier wave. Clearly, the linear approximation should fail at large time scales as the amplitude of an unstable sideband grows exponentially. Furthermore, the linear stability analysis neglects additional combination waves generated through a wave-mixing process, which, albeit small at the initial stage, can become significant at large time scales if its wave number falls in an instability domain. Linear stability analysis therefore cannot tell us the long time evolution of a modulated nonlinear plane wave. In order to check the validity of our analytical approach and to get an idea of what kind of dynamical patterns one might obtain in the system under small perturbations, we carried out numerical simulations of the DCGL equation by using the standard fourth-order Runge–Kutta method, with an integration time step of 0.055. In our numerical simulations, the initial conditions that are typically at time $t=0$, are coherently modulated plane waves of the form

$$W(t=0)=[W_0+\eta\cos(Qn)]\exp\{i[qn+0.01\cos(Qn)]\}. \tag{13}$$

Here, the amplitude parameter W_0 is obtained from Eq. (3), and the modulation amplitude is such that $\eta \ll W_0$ (η

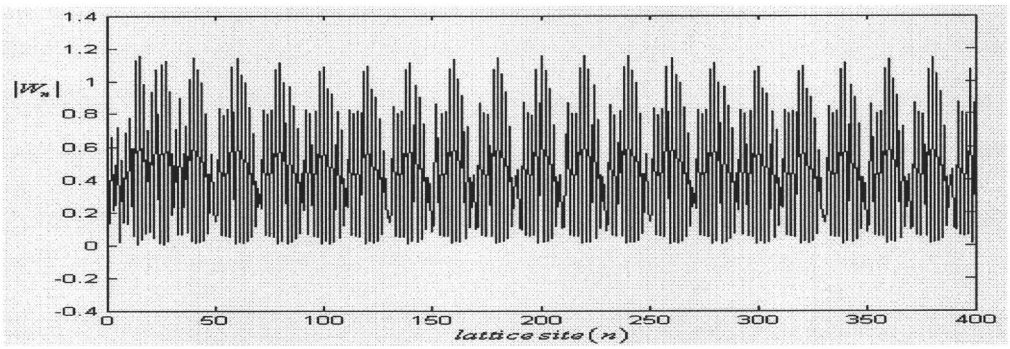

(a)

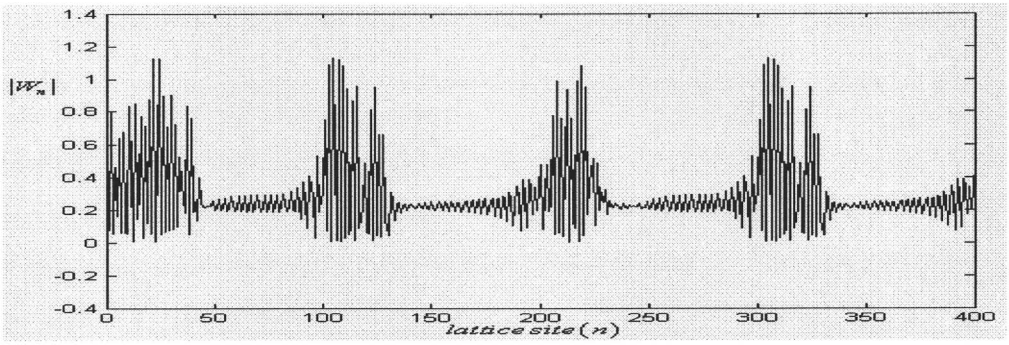

(b)

FIG. 2. Modulational instability. The same parameters as in Fig. 1(a). (a) Train of patterns with ultrashort wavelength propagating through the system at time 600 *units* and for the wave numbers $q=13\pi/20$, $Q=\pi/100$. (b) Unstable patterns with a short wavelength, at time 700 *units* corresponding to the wave numbers $q=\pi/100$, $Q=13\pi/20$.

$=W_0/100$). As a specific example, we consider a system involving N sites with $N=400$, with periodic boundary conditions. First, let us consider the case $q=13\pi/20$ and $Q=\pi/10$. That corresponds to a point labeled in Fig. 1(a) displaying the instability region in the (Q,q) plane. According to Fig. 1(a), the instability is predicted for a wave with these wave numbers. For these values of wave numbers, the initial condition is introduced in the system. One obtains an interesting phenomenon: the wave displays an oscillating and breathing wave behavior. The amplitude of the wave generated by wave motion is modulated in the form of a train of small amplitude with a short wavelength. Each component of the train has the shape of a soliton object. To illustrate this, we present in Fig. 2(a) the amplitude of the wave pattern at time 600 units. Let us consider a wave with $q=\pi/10$ modulated at a wave number $Q=13\pi/20$. The corresponding point in the (Q,q) plane in Fig. 1(a) lies in the instability region. We observe that the initial solution is also disintegrated into a train of patterns. Each element of the train also has the shape of a soliton object. But their number has drastically decreased as shown in Fig. 2(b) at time 700 units. The value of the wave number of modulation influences the number of waves oscillating with a soliton shape in the train. This phenomenon can be understood in the sense that, in this range of Q (modulated wave number), nonlinear effects in the discrete lattice lead to the creation of an extended nonlinear plane wave with a particular fact that the amplitude appears as a train of solitonlike objects. In the case of discrete electrical transmission lines, the propagation of such nonlinear wave packets has led to the observation of envelope solitons that propagate with constant velocity, and localized modes that undergo velocity fluctuations due to lattice dispersion when they propagate [32].

Figure 3 shows the time evolution of a modulated plane wave with the same parameters as those of Fig. 2. As it has been mentioned above, MI can create spatially localized patterns and modes. Stable spatially localized states have been observed experimentally in binary fluid mixtures [34], electroconvection in nematic liquid crystals [35], autocatalytic chemical reaction [36] and in granular media undergoing Faraday instability [37]. Two different mechanisms were identified to work for the localized states. The first is the feedback mechanism, which was suggested and shown to work for the quintic Ginzburg-Landau equation with a destabilizing cubic term and complex coefficients [38,39], which arises for weakly inverted bifurcations to traveling waves. While the second mechanism, namely the trapping mechanism, based on the interaction between small and large wavelengths has been suggested by Pomeau [39,40] and examined in detail for walls in Ref. [41]. Figures 3(a) and 3(b) confirm

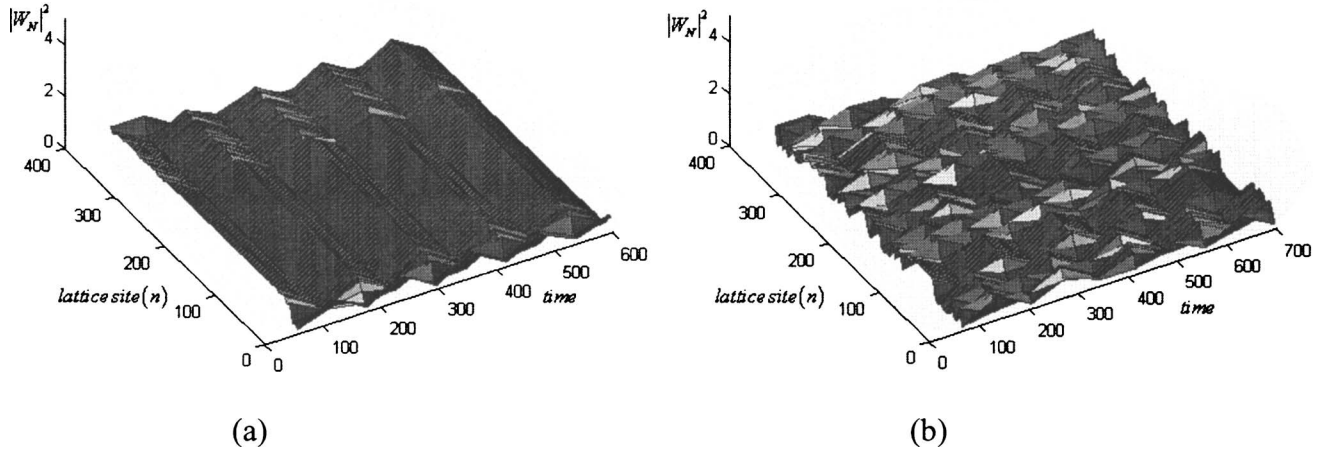

FIG. 3. Localized patterns. The same parameters as in Fig. 1(a). (a) Localized patterns at wave numbers, $q=13\pi/20$, $Q=\pi/100$. (b) Localized patterns with a different shape at wave numbers, $q=\pi/100$, $Q=13\pi/20$.

these predictions showing the creation of two types of localized patterns from a flat initial condition. To be more explicit, we display in Fig. 3(a) stable localized patterns with one shape. We observe that the prediction of instability from linear stability analysis is well recovered in this case: the principal satellite modulation Q that is considered in the initial condition produces localized patterns with one shape. On the other hand, Fig. 3(b) presents a different case, where we observe localized patterns of various sizes. We explain this special feature by the fact that, although the linear stability analysis neglects additional combination mode waves, these latter are spontaneously generated through wave-mixing processes during the propagation.

Let us now illustrate the case $q=2\pi/5$ and $Q=\pi/2$. This point lies in the stability domain in Fig. 1(a). The initial excitation may move without changing its form as coherent states. The wave pattern displayed by the set of the preceding wave number is that of a plane wave with a sinusoidal form, with a constant amplitude that is not sensitive to any modulation as the time increases. Therefore, the system is said to be stable under the corresponding modulation. This feature is described by Fig. 4(a) at time 1000 units. The wave-mixing process that has been described above is interesting because, although only one modulation wave is initially launched in the system, one notes the presence of other waves during the propagation of the main wave. We refer to the appearance of these waves as secondary waves. To illustrate this point, we present in Fig. 4(b) the spatial Fourier transform $W_n(k)$ of Fig. 4(a). Figure 4(b) presents three peaks denoting the sinusoidal character of the waves propagating in the system. The major peak is due to the initial plane wave previously introduced through the model, while the two others can be called secondary waves because they have spontaneously appeared during the propagation. In the case of modulational stability, we remark that there is no localized pattern as it is viewed in Fig. 4(c).

Coherent structures and chaotic states are well known as two distinct states of nonlinear dissipative wave systems. However, these states sometimes occur and propagate together in some systems. Thus, a coherent state and a chaotic state coexist and these two distinct structures are separated with a sheer interface [42,43]. One common feature of MI is the evolution from a single mode after a sufficiently long time into a nearly chaotic state. Therefore, numerical investigations can be used to examine the long-time evolution of a modulated extended nonlinear wave. Let us investigate this with the following model parameters: $c_0=2.1$, $c_1=-4.3$, $c_2=-0.2$, $c_3=-0.08$, $c_4=-1.2$, $\varepsilon=-0.05$, $c_1'=0.0$, $\varepsilon'=-0.016$, $\mu=1.5$, and for the wave numbers $q=\pi/14$, $Q=\pi/7$. The point labeled by this wave number lies in the instability region. But, we observe that the amplitude of the wave fluctuates randomly in space and time as its time evolution shown in Fig. 5(a). This follows because albeit linear stability analysis neglects additional combination waves generated through wave-mixing processes, these latter can become significant and drive the system in a chaotic regime if the wave numbers fall in an unstable domain. To illustrate this point, we will study the behavior of the wave with the help of the discrete spatial Fourier transform of $W_n(t)$,

$$m(p,t)=\sum_{n=0}^{N-1} W_n(t)e^{in(2p\pi/N)}, \quad \text{with} \quad -\frac{N}{4}<p\leqslant\frac{N}{4}. \tag{14}$$

The growth rate of each individual Fourier components can be obtained by the least square fitting of $|m(p,t)|^2$ over the first few periods during which time it is expected to grow. According to Fig. 5(b), the *"normally" unstable* modulation presents an exponentially increasing of the amplitude of different modes generated by the nonlinearity during the first moment. At this stage, the amplitude of these combinations decreases exponentially; then increases again until their amplitude reached the amplitude of the carrier wave. The progressive buildup of combination modes due to nonlinear coupling induces wave interactions that were not included in our linear stability analysis, and eventually all carrier waves evolve into a chaoticlike state, where all possible wavelengths are present (see Fig. 5(b) for a few of them). In this state, the amplitude of some modes becomes sometime much higher than the amplitude of the original wave. The chaoticlike state mixing all wavelengths is obtained around $t=500$ units of time.

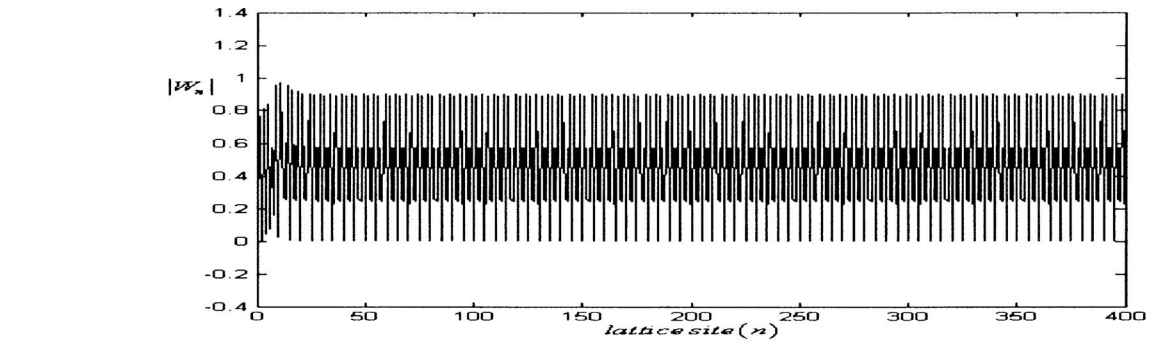

(a)

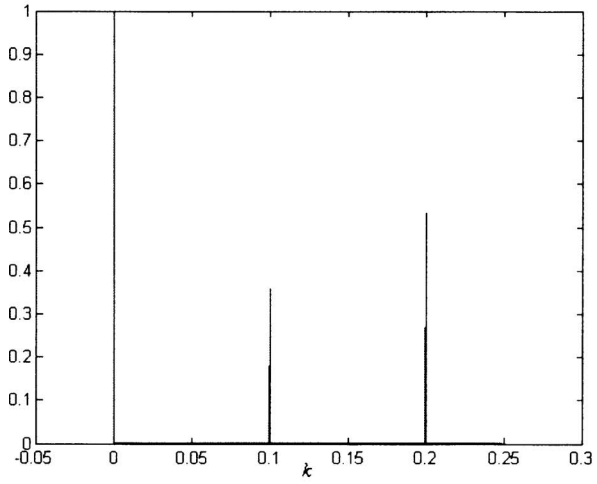

(b)

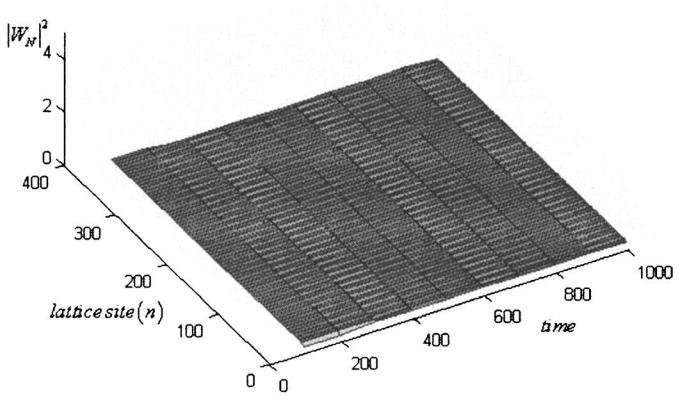

(c)

FIG. 4. Modulational stability at time 1000 *units* for the parameters. The same parameters as in Fig. 1(a). The wave numbers are $q=2\pi/5$, $Q=\pi/2$. (a) Propagation of stable patterns through the system. (b) The nonexistence of localized patterns in modulational phenomena. (c) Fourier transform of $W(k)$ corresponding to Fig. 4(a), which shows the existence of combination waves in the system.

IV. CONCLUSION

In this paper, we have investigated both analytically and numerically MI of nonlinear plane waves in a system of coupled oscillators. The perturbation of the initial solution has been considered as a combination of progressive and regressive plane waves. The frequency has been taken in its complex form where the imaginary part measures the growth rate of perturbations. The resulting dispersion relation is a fourth-order polynomial. Numerically, fairly good agreement is obtained with analytical results confirmed by the propagation of modulated patterns which have the shape of a soliton object when wave numbers lie within the unstable area of Fig. 1. Initially neglected in the linear stability analysis, combination waves appear spontaneously and lead to localized patterns. We have found that modulational instability is related to localized patterns. However, the spatiotemporal chaotic state can be crudely characterized by the fact that the amplitude evolves erratically in space [15,42]. This state arises because additional combination waves generated through wave-mixing processes drive the system in a chaotic regime. In forthcoming studies, it will be interesting to determine soliton solutions and study the origin of combination waves of this model.

ACKNOWLEDGMENTS

The authors would like to thank the Abdus Salam International Centre for Theoretical Physics (AS-ICTP).

APPENDIX: MODULATION STABILITY ANALYSIS

To investigate the modulational instability, the initial solution is perturbed in amplitude and phase. Therefore, it follows a linear and homogeneous algebraic system that arises in the form $\mathrm{Mu}=0$, with $u^{\perp}=[b_1\ \psi_1\ b_2\ \psi_2]$, where the matrix M is defined by

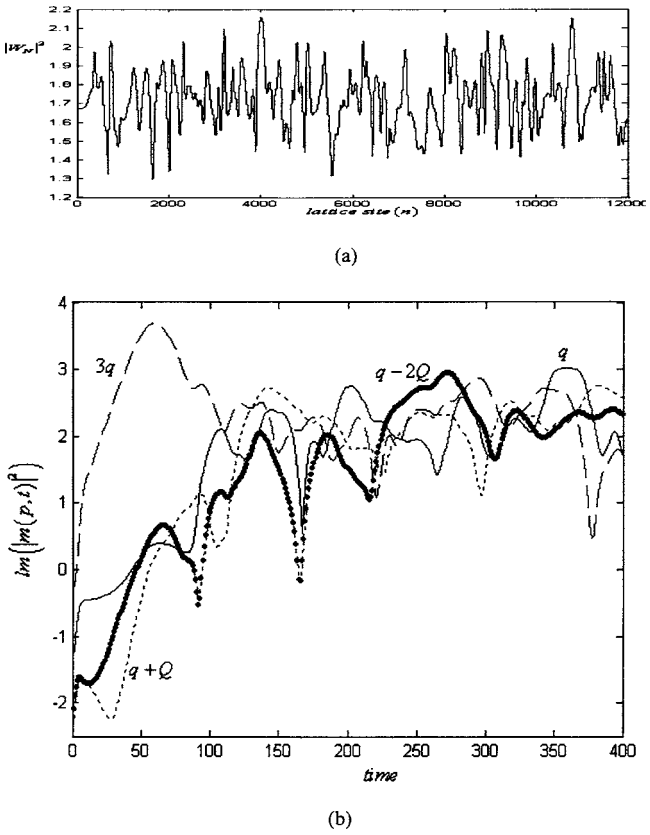

FIG. 5. Spatiotemporal chaotic states at wave numbers $q=\pi/14$, $Q=2\pi/7$, $c_0=2.1$, $c_1=-4.3$, $c_2=-0.2$, $c_3=-0.08$, $c_4=-1.2$, $\varepsilon=-0.05$, $c_1'=0$, $\varepsilon'=-0.016$, $\mu=1.5$. (a) Chaotic time evolution of $|W_N|^2$ at position $N=100$. (b) Time evolution of the amplitude of the Fourier components at wave number q (the solid line), $3q$ (dashed line), $(q+Q)$ (dotted line), and $(q-2Q)$ (dash-dotted line), for wave number $q=\pi/14$ modulated at wave number $Q=2\pi/7$. The evolution of the Fourier components shows chaotic behavior of the lattice. A logarithmic scale is used for the amplitude of the Fourier components.

$$M=\begin{bmatrix} \sigma+m_1 & m_2 & m_3 & 0 \\ m_4 & \sigma+m_5 & m_6 & 0 \\ m_7 & 0 & \sigma+m_8 & m_9 \\ m_{10} & 0 & m_{11} & \sigma+m_{12} \end{bmatrix}. \quad \text{(A1)}$$

The matrix coefficients $m_j(j=1,\ldots,12)$ are defined as follows:

$$m_1=-(1+2c_3\cos Q)W_0^2+2\varepsilon[\cos(q+Q)-\cos q]+2\varepsilon'[\cos 2(q+Q)-\cos 2q],$$

$$m_2=\Omega_r-2c_1\varepsilon[\cos(q+Q)-\cos q]-2c_1'\varepsilon'[\cos 2(q+Q)-\cos 2q],$$

$$m_3=m_7=-(1+2c_3\cos Q)W_0^2,$$

$$m_4=-\Omega_r-(c_2+2c_4\cos Q)W_0^2+2c_1\varepsilon[\cos(q+Q)-\cos q]+2c_1'\varepsilon'[\cos 2(q+Q)-\cos 2q],$$

$$m_5=2\varepsilon[\cos(q+Q)-\cos q]+2\varepsilon'[\cos 2(q+Q)-\cos 2q],$$

$$m_6=m_{10}=-(c_2+2c_4\cos Q)W_0^2,$$

$$m_8=-(1+2c_3\cos Q)W_0^2+2\varepsilon[\cos(q-Q)-\cos q]+2\varepsilon'[\cos 2(q-Q)-\cos 2q],$$

$$m_9=-\Omega_r-2c_1\varepsilon[\cos(q-Q)-\cos q]-2c_1'\varepsilon'[\cos 2(q-Q)-\cos 2q],$$

$$m_{11}=\Omega_r+-(c_2+2c_4\cos Q)W_0^2+2c_1\varepsilon[\cos(q-Q)-\cos q]+2c_1'\varepsilon'[\cos 2(q-Q)-\cos 2q],$$

$$m_{12}=2\varepsilon[\cos(q-Q)-\cos q]+2\varepsilon'[\cos 2(q-Q)-\cos 2q]. \quad \text{(A2)}$$

The following equation $Mu=0$ becomes an eigenvalue equation with a nontrivial solution, when Eq. (8) is verified. In this case, the coefficients of the dispersion relation [Eq. (8)] are written as

$$K_1=m_1+m_2+m_3,$$

$$K_2=m_5m_8+m_1m_{12}-m_4m_2+m_5m_{12}+m_8m_{12}-m_9m_{11}-m_7m_3+m_1m_5+m_1m_8,$$

$$K_3=m_5(m_8m_{12}-m_9m_{11})+m_{12}(m_1m_5-m_2m_4)+m_1(m_8m_{12}-m_9m_{11})+m_7(m_2m_6-m_3m_5)+m_8(m_1m_5-m_2m_4)+m_3(m_9m_{10}-m_7m_{12}),$$

$$K_4=m_1m_5(m_8m_{12}-m_9m_{11})+m_2m_6(m_7m_{12}-m_9m_{10})+m_3m_5(m_9m_{10}-m_7m_{12})+m_2m_4(m_9m_{11}-m_8m_{12}). \quad \text{(A3)}$$

For precise behavior of the system, we make successive transformations of the dispersion relation (8) to reach Eq. (11). The coefficients of Eq. (9), K_0', K_1', and K_2', are defined by

$$K_2'=-\frac{3}{8}K_3^2+K_2,\quad K_1'=\frac{1}{8}K_3^3-\frac{1}{2}K_2K_3,\quad K_0'=-\frac{3}{256}K_3^4+\frac{1}{16}K_2K_3^2-\frac{1}{4}K_1K_3+K_0, \quad \text{(A4)}$$

those of Eq. (11), K_0'', K_1'', are defined by

$$K_1''=-\frac{1}{3}K_2'^2-\frac{4}{3}K_0',\quad K_0''=-\frac{2}{27}K_2'^3-\frac{8}{3}K_0'K_2'-(K_1')^2. \quad \text{(A5)}$$

Solutions of Eq. (9) can be rewritten as a function of solutions $\sigma_{1(11)},\sigma_{2(11)},\sigma_{3(11)}$,

$$\sigma_1=[(\sigma_{1(11)}-2K_2'/3)^{1/2}+(\sigma_{2(11)}-2K_2'/3)^{1/2}+(\sigma_{3(11)}-2K_2'/3)^{1/2}]/2,$$

$$\sigma_2 = [-(\sigma_{1(11)} - 2K_2'/3) - (\sigma_{2(11)} - 2K_2'/3) + (\sigma_{3(11)} - 2K_2'/3)^{1/2}]/2,$$

$$\sigma_3 = [(\sigma_{1(11)} - 2K_2'/3)^{1/2} - (\sigma_{2(11)} - 2K_2'/3)^{1/2} + (\sigma_{3(11)} - 2K_2'/3)^{1/2}]/2,$$

$$\sigma_4 = [(\sigma_{1(11)} - 2K_2'/3)^{1/2} - (\sigma_{2(11)} - 2K_2'/3)^{1/2} - (\sigma_{3(11)} - 2K_2'/3)^{1/2}]/2. \quad \text{(A6)}$$

We can point out that, if one of the solutions $\sigma_{1(11)}, \sigma_{2(11)}, \sigma_{3(11)}$ is less than $K_2'/3$, the growth rate must be complex.

[1] T. B. Benjamin and J. E. Feir, J. Fluid Mech. **27**, 417 (1967).
[2] D. J. Stuart and R. C. DiPrima, Proc. R. Soc. London, Ser. A **362**, 27 (1978).
[3] L. A. Ostrovskii, Sov. Phys. JETP **24**, 797 (1969).
[4] A. Hasegawa and Y. Kodama, *Solitons in Optical Communications* (Clarendon, Oxford, 1995).
[5] T. Taniuti and H. Washimi, Phys. Rev. Lett. **21**, 209 (1968).
[6] G. P. Agrawal, *Nonlinear Fiber Optics* (Academic, San Diego, 2001).
[7] A. Hasegawa and W. F. Brinkman, IEEE J. Quantum Electron. **16**, 694 (1980); K. Tai, A. Hasegawa, and A. Tomita, Phys. Rev. Lett. **56**, 135 (1986).
[8] R. Malendevich, L. Jankovic, G. I. Stegeman, and J. S. Aitchison, Opt. Lett. **26**, 1879 (2001).
[9] H. Fang, R. Malendevich, R. Schiek, and G. I. Stegeman, Opt. Lett. **25**, 1786 (2000).
[10] D. Kip, M. Soljacic, M. Sergev, E. Eugenieva, and D. N. Christodoulides, Science **290**, 495 (2000).
[11] A. S. Davydov, J. Theor. Biol. **38**, 559 (1973).
[12] D. N. Christodoulides and R. I. Joseph, Opt. Lett. **13**, 794 (1988).
[13] W. P. Su, J. R. Schrieffer, and A. J. Heeger, Phys. Rev. Lett. **42**, 1698 (1979).
[14] A. Trombettoni and A. Smerzi, Phys. Rev. Lett. **86**, 2353 (2001).
[15] H. Willaime, O. Cardoso, and P. Tabeling, Phys. Rev. Lett. **67**, 3247 (1991).
[16] K. Otsuka, *Nonlinear Dynamics in Optical Systems* (KTK Scientific Publishers, Tokyo, 1999).
[17] D. N. Christodoulides, F. Lederer, and Y. Silberberg, Nature (London) **24**, 817 (2003).
[18] S. S. Wang and H. G. Winful, Appl. Phys. Lett. **52**, 1774 (1988); H. G. Winful and S. S. Wang, *ibid.* **53**, 1894 (1988).
[19] A. C. Newell and J. A. Whitehead, J. Fluid Mech. **38**, 279 (1969).
[20] L. A. Segel, J. Fluid Mech. **38**, 203 (1969).
[21] N. K. Efremidis and D. N. Christodoulides, Phys. Rev. E **67**, 026606 (2003).
[22] O. Cardoso, H. Willaime, and P. Tabeling, Phys. Rev. Lett. **65**, 1869 (1990).
[23] H. Willaime, O. Cardoso, and P. Tabeling, Phys. Rev. E **48**, 288 (1993).
[24] P. Tabeling, S. Fauve, and B. Perrin, Europhys. Lett. **4**, 555 (1987); P. Tabeling, O. Cardoso, and B. Perrin, J. Fluid Mech. **213**, 511 (1990).
[25] J. Meier, G. I. Stegeman, D. N. Christodoulides, Y. Silber, R. Morandotti, H. Yang, G. Salamo, M. Sorel, and J. S. Aitchison, Phys. Rev. Lett. **92**, 163902 (2004).
[26] O. M. Braun and Y. S. Kivshar, Phys. Rep. **306**, 1 (1998); D. Henning and G. P. Tsironis, *ibid.* **307**, 333 (1999).
[27] J. T. Stuart and R. C. DiPrima, Phys. Fluids **13**, 1 (1970).
[28] M. C. Cross and P. C. Hohenberg, Rev. Mod. Phys. **65**, 851 (1993).
[29] I. S. Aranson and L. Kramer, Rev. Mod. Phys. **74**, 99 (2002).
[30] Y. S. Kivshar and M. Peyrard, Phys. Rev. A **46**, 3198 (1992).
[31] J. M. Bilbault and P. Marquié, Phys. Rev. E **53**, 5403 (1996).
[32] P. Marquié, J. M. Bilbault, and M. Remoissenet, Phys. Rev. E **51**, 6127 (1995).
[33] V. I. Karpman, Pis'ma Zh. Eksp. Teor. Fiz. **6**, 759 (1967) [JETP Lett. **6**, 227 (1967)]; V. I. Karpman and E. M. Krushkal', Pis'ma Zh. Eksp. Teor. Fiz. **55**, 530 (1968) [JETP **28**, 277 (1969)].
[34] J. J. Niemela, G. Ahlers, and D. S. Cannell, Phys. Rev. Lett. **64**, 1365 (1990); P. Kolodner, *ibid.* **69**, 2519 (1992).
[35] M. Dennin, G. Ahlers, and D. S. Cannell, Phys. Rev. Lett. **77**, 2475 (1996); H. R. Brand, C. Frading, P. L. Finn, W. Pesch, and P. E. Cladis, Phys. Lett. A **235**, 508 (1997).
[36] P. de Kepper, J.-J. Perraud, B. Rudovics, and E. Dulos, Int. J. Bifurcation Chaos Appl. Sci. Eng. **4**, 1215 (1994); K. J. Lee, W. D. McCormick, J. E. Pearson, and H. L. Swinney, Nature **369**, 215 (1994).
[37] F. Melo, P. B. Umbanhowar, and H. L. Swinney, Phys. Rev. Lett. **75**, 3838 (1995).
[38] O. Thual and S. Fauve, J. Phys. (Paris) **49**, 1829 (1988).
[39] H. Sakaguchi and H. R. Brand, Physica D **117**, 95 (1998).
[40] Y. Pomeau, Physica D **23**, 3 (1986).
[41] B. A. Malomed, A. A. Nepomnyashchy, and M. I. Tribelsky, Phys. Rev. A **42**, 7244 (1990).
[42] K. Nozaki and N. Bekki, Phys. Rev. Lett. **51**, 2171 (1983).
[43] A. Kenfack Jiotsa and T. C. Kofané, J. Phys. Soc. Jpn. **72**, 1800 (2003); A. Mohamadou, A. Kenfack Jiotsa, and T. C. Kofané, Chaos, Solitons Fractals **24**, 957 (2005).